

# Chemical freeze-out in ultra-relativistic heavy ion collisions at $\sqrt{s_{NN}} = 130$ and 200 GeV.

J. Manninen

*INFN Sezione di Firenze, Florence, Italy*

F. Becattini

*Università di Firenze and INFN Sezione di Firenze, Florence, Italy*

A comprehensive and detailed analysis of hadronic abundances measured in Au-Au collisions at RHIC at  $\sqrt{s_{NN}} = 130$  and 200 GeV is presented. The rapidity densities measured in the central rapidity region have been fitted to the statistical hadronization model and the chemical freeze-out parameters determined as a function of centrality, using data from experiments BRAHMS, PHENIX and STAR. The chemical freeze-out temperature turns out to be independent of centrality to a few percent accuracy, whereas the strangeness under-saturation parameter  $\gamma_S$  decreases from almost unity in central collisions to a significantly lower value in peripheral collisions. Our results are in essential agreement with previous analyses, with the exception that fit quality at  $\sqrt{s_{NN}} = 200$  GeV is not as good as previously found. From the comparison of the two different energies, we conclude that the difference in fit quality, as described by  $\chi^2$  values, is owing to the improved resolution of measurements which has probably exceeded the intrinsic accuracy of the simplified theoretical formula used in the fits.

## I. INTRODUCTION

The idea of a statistical model to account for multiple hadron production processes in high energy collisions dates back to a work by Fermi [1]. This model has been successful in reproducing the production rates of measured hadronic species in collisions of both elementary particles [2–4] and heavy-ions [5–9]. These models have been extensively and successfully applied to the phenomenon of multifragmentation in nuclear collisions [10].

Many evidences have been collected that a new form of matter, the Quark–Gluon Plasma (QGP), where effective degrees of freedom are quarks and gluons, has been created in the collisions of heavy ions at relativistic energies at top SPS and RHIC energy. While the success of the statistical-thermal model in describing particle multiplicities indicates that local thermodynamical equilibrium has been achieved and seems to confirm the general hypothesis of QGP formation, some aspects are still to be understood, like e.g. whether strangeness is fully equilibrated and the relation of this successful description with that in elementary collisions. In this respect, an analysis of RHIC data, at a center-of-mass energies 130 and 200 GeV per colliding pair of nucleon, can be illuminating. Indeed, similar analyses have been carried out in the past few years [11–17]. Yet, recently, a bunch of new experimental data has been published which makes it a worthwhile step to provide an independent analysis including this newly available data. Furthermore, we have studied hadron production at lower beam energies in heavy-ion collisions at AGS and SPS with the statistical hadronization model [18, 19] and with this paper we complete our previous works.

There is also another issue which motivates our analysis. So far, most analyses have been using as an input to the fit  $(N - 1)$  particle ratios formed *a posteriori* from  $N$  measured particle multiplicities without including any normalizing yield. This procedure was based on the tacit assumption that fitting either ratios or multiplicities lead to equivalent results. This is in general not true and the outcome of a statistical analysis relying on *only* ratios of hadron multiplicities may be seriously biased [20], depending on the input set of ratios. The reason of this problem is that, in principle, one can form  $N(N - 1)/2$  different combinations<sup>1</sup> of particle ratios from  $N$  different measured multiplicities and choosing a subset of them implies an information loss. Moreover, the different ratios are obviously correlated if a particle appears more than once in the ratios and those correlations must be taken into account in the  $\chi^2$  minimization, thus complicating the fit. In the worst case, the central values of the fitted statistical model parameters may deviate several standard errors from the central values of parameters determined from a fit to particle multiplicities whereas the actual magnitude of the error is not possible to know without explicit comparison. We stress that this problem arises when using ratios calculated *a posteriori* from a set of primordially measured multiplicities, while ratios directly measured by the experiments because of beneficial systematic error cancellation (e.g.  $\pi^-/\pi^+$  or  $\bar{p}/p$ ) are perfectly safe.

While at lower beam energies integrated multiplicities in full phase space are a more suitable input for the statistical

---

<sup>1</sup> counting  $A/B$  and  $B/A$  equivalent

model [18], at RHIC energies of  $\sqrt{s_{\text{NN}}} > 100$  GeV, rapidity distributions are wide enough to allow the extraction of the thermodynamical properties of the average fireball produced at mid-rapidity with rapidity densities themselves. In fact, the standard width of charged particle rapidity distribution at  $\sqrt{s_{\text{NN}}} = 200$  GeV is 2.1 [21], sufficiently larger than standard widths of single-fireball rapidity distribution (at most 0.8 for pions at the kinetic freeze-out temperature of 125 MeV). On the other hand, at top SPS energy  $\sqrt{s_{\text{NN}}} = 17.2$  GeV the measured rapidity width is 1.3 [22], which is consistently smaller and closer to the single-fireball width. Therefore, using mid-rapidity densities at this and lower energies artificially enhances heavier particles with respect to lighter ones as they have a narrower rapidity distribution.

## II. THE DATA ANALYSIS

We have analyzed the rapidity densities in Au-Au collisions at 130 and 200 GeV per participating nucleon measured by BRAHMS, PHENIX and STAR collaborations at RHIC employing a version of statistical hadronization model described in detail in [18, 19]. The use of the grand-canonical formalism is appropriate here in that particle multiplicities are large. The formula for the  $i$ th primary hadron (including both stable hadrons and resonances) rapidity density reads:

$$\left\langle \frac{dn_i}{dy} \right\rangle = \frac{dV}{dy} \frac{(2J_i + 1)}{(2\pi)^3} \int d^3p \left[ \gamma_S^{-n_{si}} e^{\sqrt{p^2 + m_i^2}/T - \boldsymbol{\mu} \cdot \mathbf{q}_i/T} \pm 1 \right]^{-1} \quad (1)$$

where  $T$  is the temperature,  $\mathbf{q}_i = (Q_i, B_i, S_i)$  is a vector having as components the electric charge, baryon number and strangeness of the hadron and  $\boldsymbol{\mu} = (\mu_Q, \mu_B, \mu_S)$  is a vector of the corresponding chemical potentials;  $\gamma_S$  is the strangeness under-saturation factor and  $n_{si}$  is the number of valence strange quarks in the  $i$ th hadron; the upper sign applies to fermions, the lower to bosons. The absolute normalization  $dV/dy$  in (1) is a product of the rapidity density of clusters at mid-rapidity  $\rho(0)$  times the volume of the average fireball at mid-rapidity [19]. For the above formula to make sense, the parameters  $T$ ,  $\boldsymbol{\mu}$  and strangeness under-saturation factor  $\gamma_S$  should be constant over a rapidity range encompassing the single fireball rapidity width [19]. In this work, the chemical potential  $\mu_S$  is determined enforcing vanishing strangeness density and  $\mu_Q$  by requiring the final ratio of charge to baryon number to equalize the initial one  $Z/A$ , i.e. by assuming that there is no major dependence of the strangeness and electric density on rapidity. The other 4 parameters ( $T, \mu_B, \gamma_S, dV/dy$ ) are determined by minimizing the  $\chi^2$ :

$$\chi^2 = \sum_i \frac{(dN_i^e/dy - dN_i^t/dy)^2}{\sigma_i^2} = \sum_i \frac{(dN_i^e/dy - n_i^t dV/dy)^2}{\sigma_i^2} \quad (2)$$

in which  $dN_i^e/dy$  and  $dN_i^t/dy$  are the experimental and theoretical rapidity densities,  $n_i^t$  is the particle density evaluated within statistical hadronization model and  $\sigma_i$  is the experimental error of the rapidity density of a particle species  $i$ . Unless otherwise stated, all experimental errors quoted in this paper are a quadratic sum of statistical and systematic errors. Before going deeper into the data analysis and exploration of results, we need to discuss a preliminary treatment of the experimental data which was necessary to make a combined analysis of all experiments.

### A. Centrality interpolations

Particle rapidity densities are measured in some selected centrality windows which are different for different experiments. As a consequence, measurements relevant to e.g. the most central collisions from different experiments must be renormalized. Moreover, the chosen centrality windows can be different for different particle species even within the same experiment. Therefore, in order to make a correct analysis of the full data set, one needs to find a proper method to estimate rapidity densities of different hadronic species *in the same centrality* window, i.e. a proper interpolation method. This can be done in many ways. For example, taking advantage of a possible linear and parabolic scaling with number of participants ( $N_{\text{P}}$ ) or number of binary collisions ( $N_{\text{bin}}$ ) as well as with the negative hadron pseudo-rapidity density ( $dN_{\text{h}^-}/d\eta$ ). In many cases such a simple scaling behaviour can be found. For example, STAR collaboration has found out [23] that  $\Lambda$  and  $\bar{\Lambda}$  rapidity densities scale well with the  $dN_{\text{h}^-}/d\eta$  in Au-Au collisions at 130A GeV. However, none of the above-mentioned scaling variables with simple functional forms is able to describe the centrality dependence of all different hadron species; instead, more complex dynamical combination (e.g. [24, 25]) of “hard” and “soft” physics processes must be considered.

Typically the interpolation correction is not very large. For instance, we might want to estimate the rapidity density of a hadron species in the [0-6%] most central collisions while the experimental value is given for the [0-5%] and [5-10%]

most central collisions. It is also important to note that centrality fractions are independent of the observable used to define them provided that the observable varies monotonically; this ensures the one-to-one correspondence between different observables. We have chosen an interpolation method we deem is more robust and model-independent than any simple scaling with  $N_P$ ,  $N_{\text{bin}}$  or  $dN_{h^-}/d\eta$  and implemented it consistently for all<sup>2</sup> rapidity densities that need to be interpolated. We write the rapidity density of a hadron species  $i$  as a  $k_{\text{max}}$ th order polynomial of the centrality as follows:

$$\frac{d^2 N_i}{dydc} = \sum_{k=0}^{k_{\text{max}}} \alpha_k^i c^k \quad ; \quad c = 1 - x \quad (3)$$

in which  $\alpha_k^i$  denote free parameters and  $x \in [0, 1]$  is the fraction of the differential cross section as a function of the variable defining centrality itself (0=0% most central and 1=100% most central collisions). The rapidity density of a hadron species in a certain centrality window  $[y_{\text{min}}, y_{\text{max}}]$  is obtained by integrating Eq. (3) over  $[y_{\text{min}}, y_{\text{max}}]$ . We thereby calculate the rapidity densities in the centrality windows where they have been measured and fit the  $k_{\text{max}}+1$  free parameters to reproduce the measured rapidity densities. Once the parameters are fitted, rapidity densities of any hadron species can be estimated in any centrality window  $[y'_{\text{min}}, y'_{\text{max}}]$  by simply integrating with respect to  $c$  over the desired region of centrality keeping the fitted parameters fixed. The maximal order of the polynomial (i.e. maximal number of free parameters minus one) for a certain particle species  $i$  is the number of centrality bins in which it is measured. We have always chosen the maximal order  $k_{\text{max}}=N_{\text{windows}}-1$  for these interpolations unless<sup>3</sup> this would lead to non-monotonic behaviour of Eq. (3) within the centrality range we are interested in, in which case we have chosen the maximal order such that the polynomial is monotonically increasing. The original experimental errors are properly propagated so that the errors of our interpolated rapidity densities include the original errors as well as the additional uncertainty arising from the interpolation.

An example of our interpolations is shown in fig. 1. In the left panel,  $\Lambda$  (open round symbols) and  $\bar{\Lambda}$  (open square symbols) rapidity densities measured by STAR collaboration at 130A GeV are shown while the filled symbols denote our estimates for the corresponding rapidity densities in 7 other centrality windows, namely the ones in which kaons and nucleons are measured. In the right panel of fig. 1, similar plot is shown for  $\Xi^-$  and  $\Xi^+$  at 200A GeV.

The experimental rapidity densities as well as our interpolated values are shown in tables I, II and III. The numbers in plain text are our estimates while numbers written in bold case are the experimental values our interpolations are based on.

## B. Au-Au collisions at 130A GeV

STAR collaboration has measured  $p$  [26],  $\bar{p}$  [26],  $K^+$  [27] and  $K^-$  [27] rapidity densities around mid-rapidity in Au-Au collisions at 130A GeV in 8 centrality bins, see table I. Proton and anti-proton rapidity densities include weak feeding from (multi)strange hyperons. We have chosen to perform our statistical model analysis as a function of centrality at this beam energy in the centrality windows nucleons and kaons are measured.

On the other hand,  $\Lambda$  and  $\bar{\Lambda}$  rapidity densities are measured in 5 different centrality bins [23] and the rapidity densities also include weak feeding from multi-strange hyperons. By fitting different functions to the transverse mass spectra, STAR collaboration has obtained two slightly different values for both  $\Lambda$  and  $\bar{\Lambda}$  rapidity densities, thus we have taken a weighted average of those. Since  $\Lambda$  and  $\bar{\Lambda}$ 's centrality bins differ somewhat from the centrality bins in which nucleons and kaons are measured, we have estimated the hyperon yields in the latter ones as described in the previous section.

For the fit to be reliable, it is necessary to include the most abundantly produced particles, charged pions, in the analysis. However, the integrated STAR  $\pi^\pm$  rapidity densities (corrected for weak decay feeding) are publicly available only in the 0-5% most central bin at 130A GeV [28] and so polynomial interpolation for peripheral collisions can not be implemented. Without better knowledge, we have assumed that the ratio

$$\frac{dN_{\pi^+}}{dy} / \frac{dN_{h^-}}{d\eta} = \frac{dN_{\pi^-}}{dy} / \frac{dN_{h^-}}{d\eta} = 239.0/296.6 \quad (4)$$

retains its value in every centrality bin. Since most of the charged hadrons emitted in a heavy-ion collision are pions, we deem that Eq. (4) yields a reasonable estimate of the pion rapidity densities. As far as the error on the estimated

<sup>2</sup> there are few exceptions to this rule which will be explicitly discussed

<sup>3</sup> this happened in one case

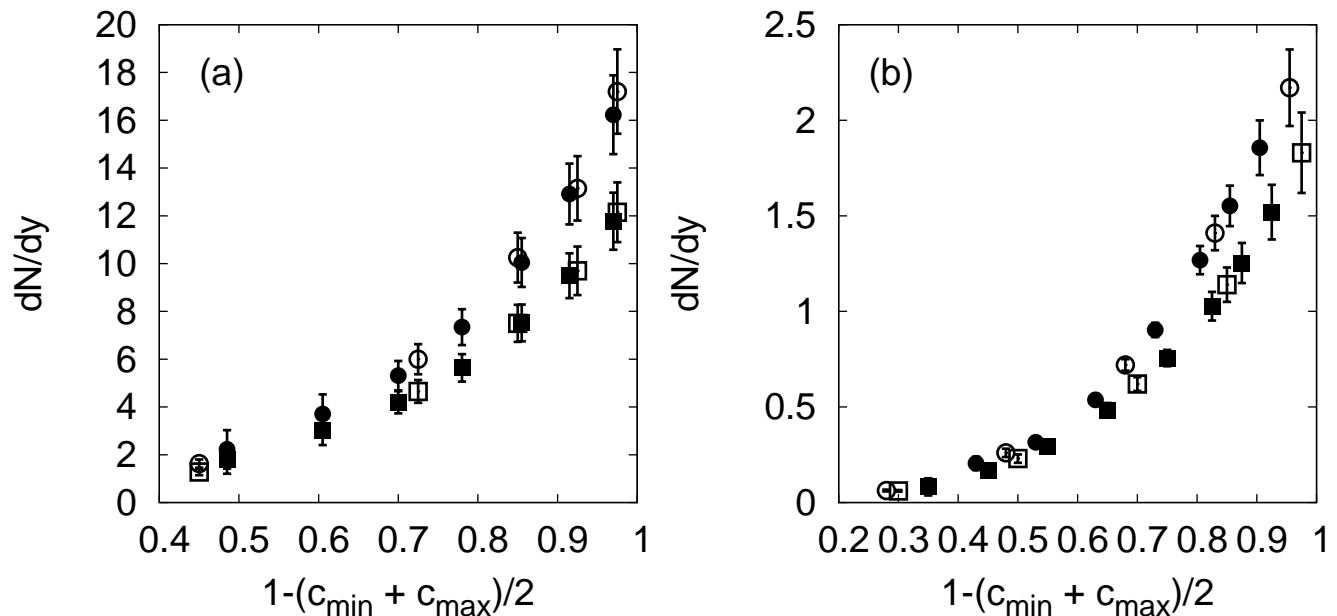


FIG. 1: Left panel (a): Experimental  $\Lambda$  (open round symbols) and  $\bar{\Lambda}$  (open square symbols) rapidity densities as a function of centrality ( $c_{\min}$  and  $c_{\max}$  being the borders of the centrality window under consideration) in Au-Au collisions at 130A GeV measured by STAR collaboration [23]. Full symbols denote our interpolated rapidity densities in centrality windows the statistical analysis is carried out.

Right panel (b): Measured  $\Xi^-$  (open round symbols) and  $\Xi^+$  (open square symbols) rapidity densities in Au-Au collisions at 200A GeV [17]. The full symbols denote our estimates for the same rapidity densities in the centrality windows the statistical analysis is carried out. The round symbols are shifted 0.02 leftward for clarity.

$c_{\min}$  and  $c_{\max}$  denote the limits of the centrality bin corresponding to each data point; in other words, the data points have been stick in the centre of the bin.

rapidity densities is concerned, we have added the additional systematic error arising from the extrapolation to different centrality bins in quadrature with the relative error of 4.5% that is quoted in the 0-5% most central collisions. Based on the published [23, 27] systematic errors of  $dN_{h^-}/d\eta$  in the various centrality bins, we estimate an overall error of 10.3% in the pion rapidity density. In order to check the stability of our analysis, we have repeated the fits by assuming 5% and 15% error in the pion rapidity densities in each centrality bin. The ensuing fitted parameters showed little difference and their central values turned out to be well within the error bar of the main fit.

The rapidity densities of hyperons  $\Xi^-$  and  $\Xi^+$  have been measured in 3 centrality windows (0-10%, 10-25% and 25-75% most central collisions) while  $\Omega + \bar{\Omega}$  is measured in the 0-10% most central collisions [29] only. Similarly to  $\Lambda$  and  $\bar{\Lambda}$ , two slightly different rapidity densities are quoted for both  $\Xi$ 's and we have taken the weighted average as our input for the analysis. Finally,  $\phi$ -meson is measured in 3 different centrality windows (0-11%, 11-26% and 26-85% most central collisions) [30]. Similarly to  $\Lambda$ 's, we have estimated the  $\Xi^\pm$  and  $\phi$  rapidity densities in the 8 STAR reference centrality bins, but since data is available in 3 centrality windows only, a 2nd order interpolation polynomial was used in Eq. (3).

Because of the vast width of the peripheral centrality window ( $\approx 30 - 80\%$  most central collisions), our method to estimate  $\Xi$  and  $\phi$  rapidity densities fails in the most peripheral bin (58-85%), and in general the relative errors increase with decreasing centrality. Particularly, the extrapolation of  $\Omega + \bar{\Omega}$  rapidity density from central to peripheral collisions based on a single centrality is meaningless. Thus, we have removed  $\Omega$  from the STAR particle set to estimate the freeze-out parameters in Au-Au collisions at 130A GeV in the 7 most central bins. As a check, the analysis has been repeated in the two most central bins by including  $\Omega + \bar{\Omega}$  rapidity density, which we have assumed to scale with the negative hadron pseudo-rapidity density, at least in this short range. The fit outcome turns out to be essentially unaffected by this inclusion and thus all quoted results in this work at 130A GeV refer to fits without  $\Omega$ 's.

Also PHENIX collaboration has measured  $\pi^+$ ,  $\pi^-$ ,  $K^+$ ,  $K^-$ ,  $p$  and  $\bar{p}$  rapidity densities in a pseudo-rapidity window of  $|\eta| < 0.35$  around mid-rapidity in Au-Au collisions at 130A GeV [31, 32]. The data is divided in 5 centrality bins (see table I) which differ from STAR's ones and thus direct comparison is not possible. Also,  $\Lambda$  and  $\bar{\Lambda}$  rapidity densities have been measured in the most central bin at 130A GeV [33]. No weak decay corrections were applied to

any of the hadron species. We have repeated the fits with the PHENIX data and found out that the data set is rich enough to fix all the statistical model free parameters only in the most central bin, in which hyperons are included in the data sample (see fig. 2 and table IV). In the other bins, the set  $\pi^\pm$ ,  $K^\pm$ ,  $p$  and  $\bar{p}$  does not allow to reliably fit all the 4 free parameters because of the relatively short lever arm in mass and the low baryon chemical potential which makes pions multiplicities too close.

Finally, we have made a combined fit to PHENIX and STAR data. First, the PHENIX rapidity densities of  $\pi^\pm$ ,  $K^\pm$ ,  $p$  and  $\bar{p}$  have been estimated in the STAR centrality bins (see again table I) according to the aforementioned interpolation procedure. The obtained  $K^\pm$  and nucleon rapidity densities agree very well with the corresponding experimental STAR values in the most central bin while the relative discrepancy increases in the more peripheral ones, yet within the error bars. It should also be pointed out that PHENIX rapidity densities of pions are larger than the corresponding STAR values because in the former case no weak decay corrections was applied. The possible different overall normalization between the 2 experiments was taken into account by introducing one more free parameter  $f_P$  multiplying all PHENIX rapidity densities; otherwise stated, the common scaling factor  $dV/dy$  becomes  $f_P \times dV/dy$  for PHENIX data. Obviously, one expects  $f_P \approx 1$  in each centrality bin, if the experiments are to be in essential agreement.

The statistical model best fit parameters determined from the combined STAR+PHENIX fit are shown in fig. 2 and table IV along with those determined by a fit to STAR data alone. It can be seen that they are in very good agreement with each other and that the cross-normalization parameter  $f_P$  varies between 0.8 to 0.92 throughout the examined centrality range.

### C. Au-Au collisions at 200A GeV

The analysis has been carried out also at  $\sqrt{s_{NN}} = 200$  GeV. At this energy, PHENIX collaboration has measured [34] the rapidity densities of the same set of hadrons as at  $\sqrt{s_{NN}} = 130$  GeV, i.e.  $\pi^\pm$ ,  $K^\pm$ ,  $p$  and  $\bar{p}$  over 11 centrality bins. Pion rapidity densities do not include weak decay products while proton and anti-proton rapidity densities are corrected from  $\Lambda$  and  $\bar{\Lambda}$  feeding. Like at the lower beam energy, the set of different hadron species is not large enough for us to fit the statistical model parameters reliably.

STAR collaboration has measured the same hadron species ( $\pi^\pm$ ,  $K^\pm$ ,  $p$ ,  $\bar{p}$ ,  $\Lambda$ ,  $\bar{\Lambda}$ ,  $\phi$ ,  $\Xi^\mp$  and  $\Omega + \bar{\Omega}$  [12, 17, 35, 36]) as at  $\sqrt{s_{NN}} = 130$  GeV. The centrality windows in which STAR and PHENIX have measured pions, kaons and protons are mostly the same. In order to minimize the amount of data manipulation, we have chosen to keep the PHENIX data as it is and to estimate STAR rapidity densities, whenever necessary, in PHENIX centrality bins. The hyperons and  $\phi$  meson have been measured in many more centrality windows than at the lower beam energy. Still, most of the windows are wider than the ones for pions and so we have interpolated hyperon rapidity densities in the narrower pions centrality windows according to Eq. (3). All rapidity densities measured by STAR collaboration are cleaned from weak decay products except  $p$  and  $\bar{p}$  which include feeding from hyperons.

Finally, BRAHMS collaboration has measured the same hadron rapidity densities [37] as PHENIX collaboration in 4 different centrality windows. The pion rapidity densities do not include any weak decay products while only  $\Lambda$  and  $\bar{\Lambda}$  decay products are subtracted from nucleon rapidity densities. We have estimated the BRAHMS rapidity densities in the same centrality bins defined by PHENIX collaboration.

Similarly to the lower beam energy, we have determined the chemical freeze-out parameters by performing a fit to STAR data alone and then a combined fit to STAR, PHENIX and BRAHMS rapidity densities. In the combined fit, free parameters  $f_P$  and  $f_B$  multiplying theoretical rapidity densities of PHENIX and BRAHMS respectively have been introduced in order to take into account possible discrepancy in overall normalization among different experiments. As it seems that there is a significant discrepancy in the  $\Lambda/p$  among the three experiments, we have decided to exclude proton and anti-proton rapidity densities measured by PHENIX and BRAHMS collaborations in the analysis (see detailed discussion in Section III). The resulting statistical model best fit parameters are shown in table V and fig. 3.

### D. Further notes

We have left out from our analysis some additional rapidity densities of hadron species that are measured at RHIC. The PHENIX measurement [38] of  $\phi$  meson at 200A GeV is left out from our analysis due to the very large discrepancy with the corresponding STAR values. We have compared the statistical model predictions for  $\phi$  meson production with the PHENIX measurement though, and found out a severe disagreement between the statistical model prediction and the PHENIX measurement (of the same order as between STAR and PHENIX measurements).

Also, STAR measurements [39, 40] of strange resonances  $K(892)$ ,  $\Sigma(1385)$  and  $\Lambda(1520)$  are left out from our analysis due to their very short lifetime which makes their decay products rescatter after chemical freeze-out, a known issue

(see e.g. [18]) in statistical model analysis *in heavy-ion collisions*. On top of above measurements, we have omitted the STAR  $K_S^0$  [27] measurement in our analysis. Within the statistical hadronization model,  $K_S^0$  multiplicity is always between the  $K^+$  and  $K^-$  yields while the STAR measurement suggests much smaller  $K_S^0$  multiplicity compared with both  $K^+$  and  $K^-$ . Thus, in this case statistical hadronization model would not be able to reproduce all  $K$  rapidity densities on a satisfactory level and so we have decided to rely on the  $K^\pm$  yields only. In order to take into account the additional uncertainty on parameters implied in fits with  $\chi^2/dof > 1$ , parameter errors have been rescaled by  $\sqrt{\chi^2/dof}$  if this is larger than 1, according to Particle Data Group procedure [41].

### III. DISCUSSION

Looking at the figs. 2 and 3, the most striking feature of statistical hadronization model fits is that temperature and baryon-chemical potential do not show much dependence on centrality. Particularly, temperature is constant at few percent level. The strangeness phase-space under-saturation parameter  $\gamma_S$  seems to be somewhat smaller than unity in peripheral collisions but reaches unity in semi-central collisions and then saturates. All of this is in agreement with previous findings [14, 17]. Indeed, the increasing trend of  $\gamma_S$  as a function of centrality is more evident at 130 GeV than at 200 GeV; furthermore, at 130 GeV  $\gamma_S$  apparently exceeds 1 in the most central collisions. However, given the large error bar, this parameter is still consistent with its natural saturation value, i.e. 1. With the present level of accuracy, we believe that no claim can be made about different values of  $\gamma_S$  at the two energies.

Comparing the statistical hadronization model parameters among the two different beam energies with the same  $N_P$ , we see very little differences. The resulting chemical freeze-out temperatures,  $\gamma_S$  factors and scaling volumes are very similar and we can see mild beam energy dependence in the baryon chemical potential only. Thus, it seems that at RHIC energies we have reached a saturation limit in which hadrons decouple from the strongly interacting system at mid-rapidity in almost the same thermodynamical state. We then easily predict, in agreement with others, that Pb-Pb collisions at the LHC will find  $T \approx 170$  MeV and  $\gamma_S \approx 1$ .

The statistical hadronization model describes the STAR data very well at 130A GeV in every centrality bin. The  $\chi^2/dof$  is less than 1 (see table IV and fig. 2) both with STAR data alone as well as with the combined STAR + PHENIX data. The resulting cross normalization factors  $f_P$  in the combined fit are around 0.9 in the central and semi central collisions while in the peripheral systems we find rather low factors of the order of 0.8. The same tendency is already visible when comparing the experimental STAR rapidity densities and our interpolated PHENIX rapidity densities at 130A GeV. Up to what extent this is a manifestation of a true difference in absolute normalization among these two experiments in peripheral collisions or a fit artefact is not possible to decide based on the published data available because there is no overlap in the particle sample. At this energy, it seems that statistical hadronization model tends to overestimate the proton and anti-proton rapidity densities while other particle species are very well described and no systematic discrepancy is seen between data and model.

Conversely, at  $\sqrt{s_{NN}} = 200$  GeV, the  $\chi^2/dof$  values (see table V and fig. 3), are larger than one. This is simply due to the better accuracy of measurements at the larger beam energy while the average relative deviations of calculated rapidity densities from the experimental ones are of the same order at both energies (in fact, they are 9.7% and 11.5% in central heavy-ion collisions at 130A GeV and 200A GeV respectively). The residuals (defined as the ratio between the difference model-data and the experimental error) and relative deviations of measured and calculated rapidity densities in central Au-Au collisions at 130 and 200A GeV are shown in tables VI and VII where one can see that the model is able to reproduce the data at the same level of accuracy at both beam energies.

For this reason, it should be stressed that the  $\chi^2$  test should be used very carefully in order to avoid naive and hasty judgements about the validity of the model. Indeed, what these values at different energies tell us is that the simple formula (1) is valid up to some level of resolution and fails when the accuracy of measurements exceeds it, i.e. at 200A GeV. This is really no surprise because formula (1) relies on several side-assumptions and approximations that are not expected to be exactly fulfilled. In other words, the theoretical model expressed by (1) is to be taken as a zero-order approximation and not as a precise representation of the real process. When the resolving power of experiments is good enough, higher order corrections become necessary, although they are very difficult to estimate and implement. For instance, an assumption which may not be exactly true is the vanishing of strangeness density at mid-rapidity, which has been used in our fits; clearly, treating  $\mu_S$  as a further free parameter could reduce the  $\chi^2$ . Another important approximation is concerned with the hadron-resonance gas model, where both hadrons and resonances are handled as free particles with distributed mass and the contribution of non-resonating interactions among stable hadrons is neglected; it is clear that this approximation will fail at some very good resolution. Finally, it should be reminded that the sharp separation between chemical and kinetic freeze-out is also an idealization. Even though hadronic rescattering does not play a major role in determining particle abundances (one good evidence is the success of the statistical model itself), we know that it is there; thus, different inelastic reactions may cease at different stages of the post-hadronization expansion and this involves deviations from the simple scheme of elastic-inelastic separation.

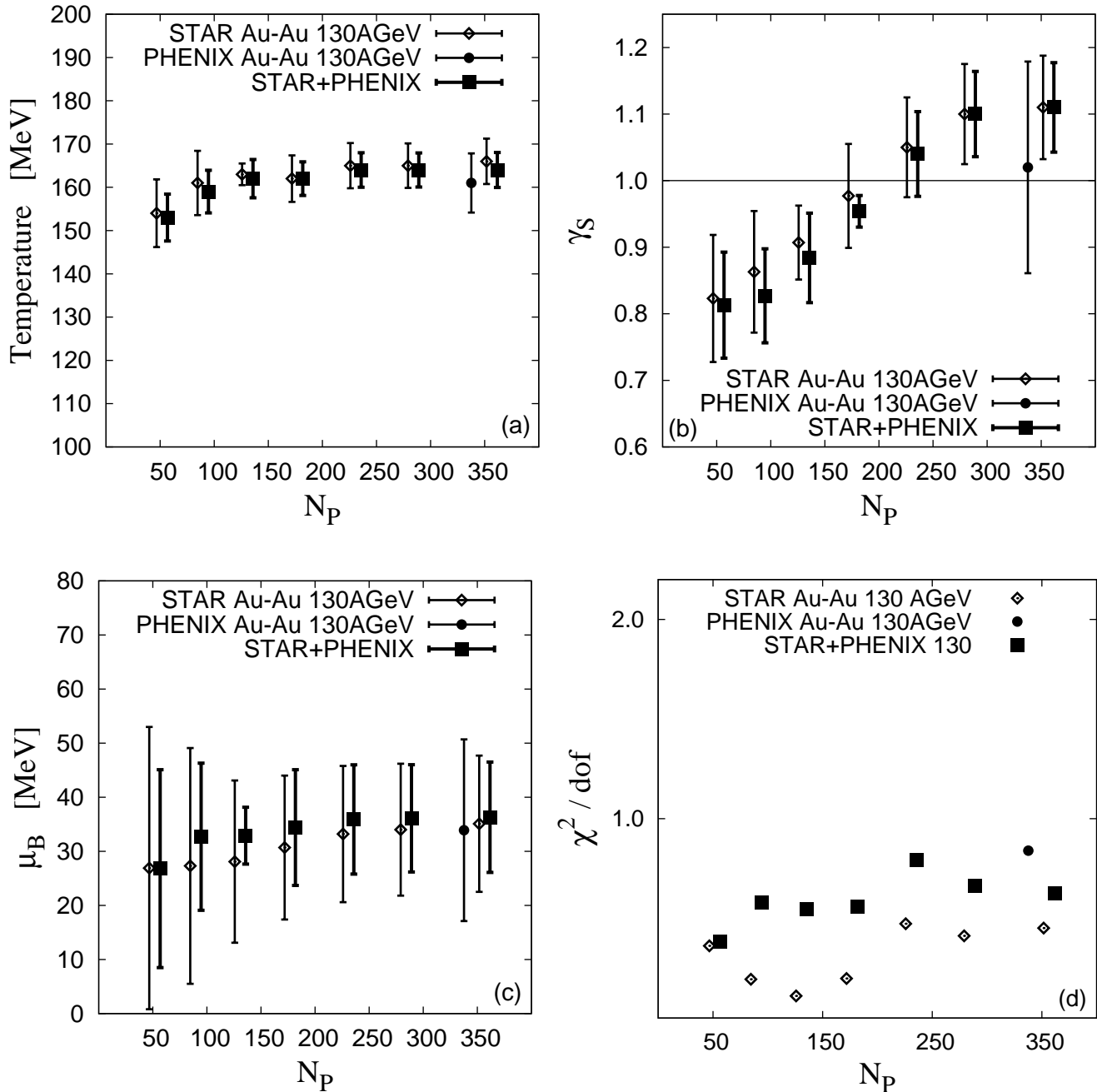


FIG. 2: Chemical freeze-out temperature (top left panel (a)), strangeness under-saturation parameter  $\gamma_s$  (top right panel (b)), baryon chemical potential (bottom left panel (c)) and the best fit  $\chi^2$  per degrees of freedom (bottom right panel (d)) as a function of collision centrality in Au-Au collisions around mid-rapidity at 130A GeV. Open symbols represent fits to STAR data while square full symbols represent fits to combined STAR+PHENIX data and the full round symbol a fit to PHENIX data alone. The full square symbols are shifted 10 units rightward and the full round symbol 10 units leftward for clarity.

Nevertheless, the  $\chi^2$  fit is a useful tool to determine the best parameters of the zero-order theory but should be used with care as an absolute measure of the fit quality. For example, the relative errors of hadron multiplicities in  $e^+e^-$  experiments are typically few percent only, which leads to relatively large  $\chi^2/dof$  values [42] at least when compared with the  $\chi^2/dof$  values in heavy-ion collisions in which the relative errors of multiplicities are typically larger and thus a blind comparison of the  $\chi^2/dof$  values arising from the fits to elementary collisions and heavy-ion collisions could be highly misleading. However, as has been mentioned, if fits have a low quality, the estimated parameter errors

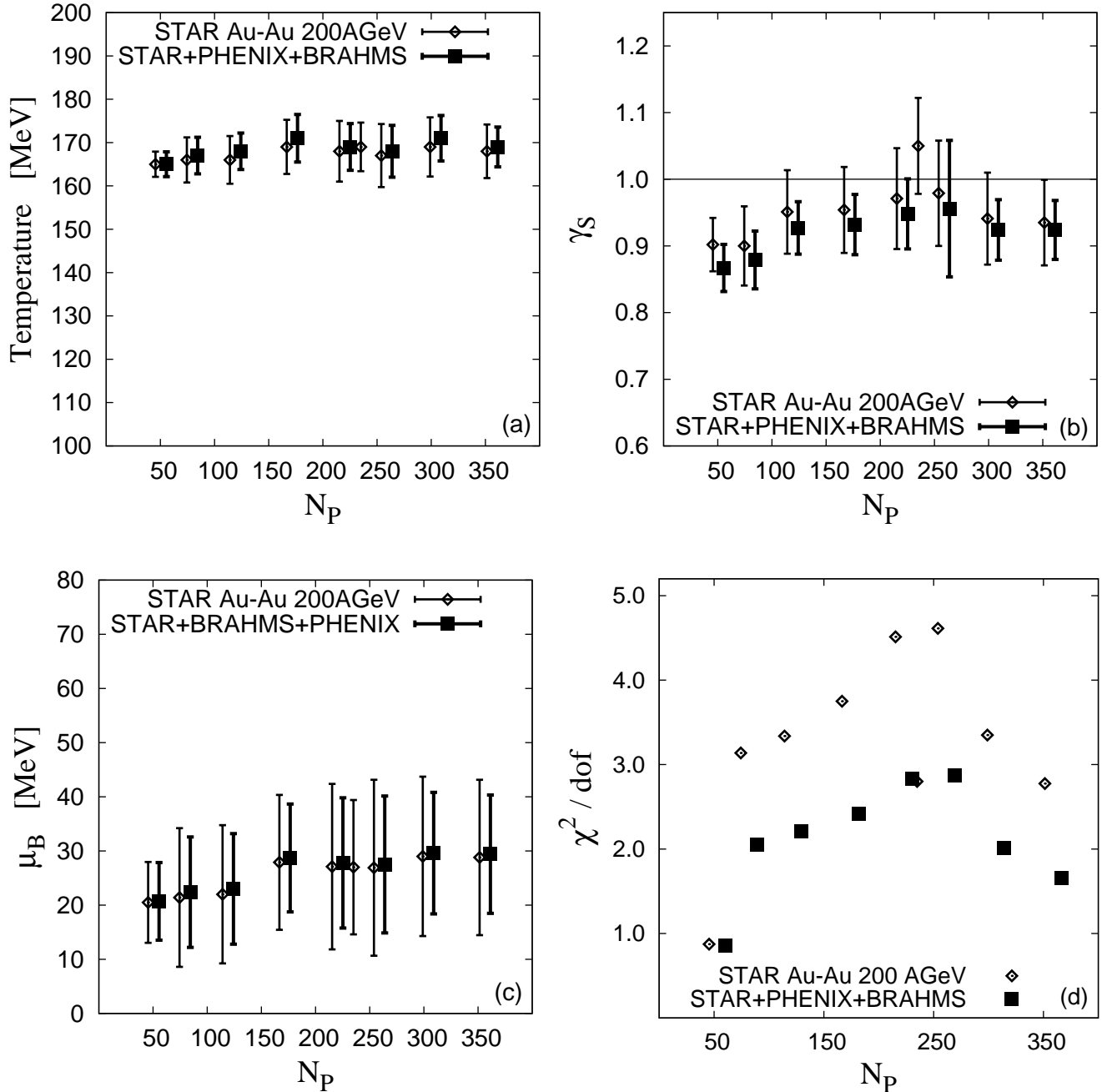


FIG. 3: Chemical freeze-out temperature (top left panel (a)), strangeness under-saturation parameter  $\gamma_s$  (top right panel (b)), baryon chemical potential (bottom left panel (c)) and the best fit  $\chi^2$  per degrees of freedom (bottom right panel (d)) as a function of collision centrality in Au-Au collisions around mid-rapidity at 200A GeV. Full symbols represent fits to combined STAR+PHENIX+BRAHMS data while the open symbols represent fits to STAR data only. The filled symbols are shifted 10 units rightward for clarity.

could be unrealistically small and this is why we rescaled errors by  $\sqrt{\chi^2/dof}$ , according to the procedure adopted by Particle Data Group in such cases [41].

Fits to STAR data at 200A GeV do not reveal any particular discrepancy between the experiment and the model, all particle species are roughly equally well described ( $\sim 1\sigma - 2\sigma$  deviation) with the exception of pions which are always very well reproduced (see fig. 4). We have repeated the fits by systematically removing different particle species from the fits and found out that similarly to the lower beam energy, statistical model seems to have problems

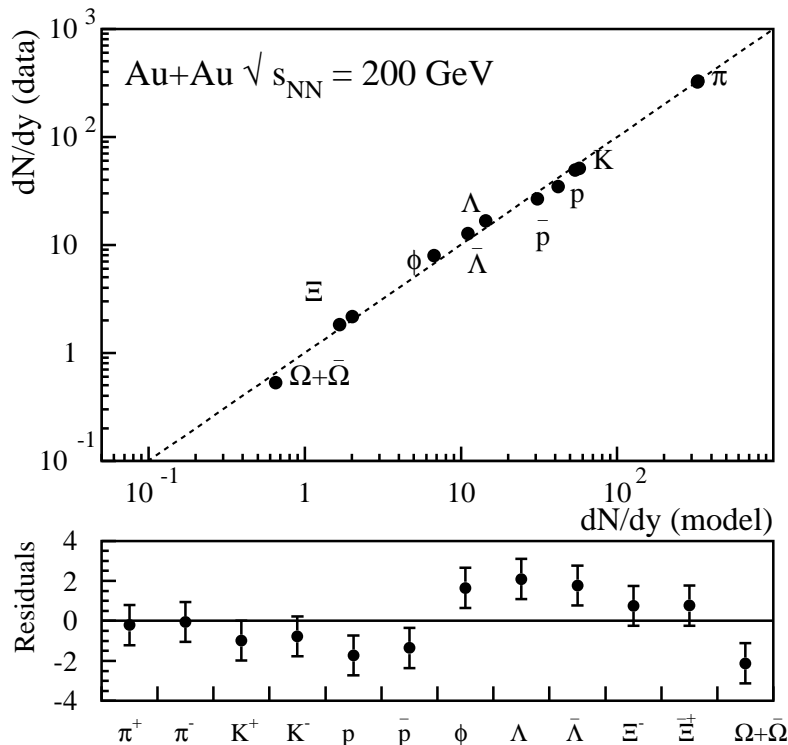


FIG. 4: Above: measured versus fitted rapidity densities in Au-Au collisions at  $\sqrt{s_{NN}} = 200$  GeV. Below: residual (defined here as the ratio between the difference data-model and the experimental error) distribution. The data is from STAR, the model values refer to the combined fit to BRAHMS, STAR, PHENIX experiments.

in reproducing the proton and anti-proton rapidity densities especially together with the  $\Lambda$  and  $\bar{\Lambda}$  rapidity densities. Removal of either of these two particle species (and their antiparticles) will lead to much smaller  $\chi^2/dof$  values while the resulting best fit parameters are adjusted within the errors of the parameters resulting from a fit to the full data set. In general, the statistical hadronization model tends to systematically over estimate the  $\Omega + \bar{\Omega}$  rapidity density and under estimate the other hyperon yields at 200A GeV.

Fits to the combined STAR+PHENIX+BRAHMS data shed further light to the issue of short lever arm of the PHENIX and BRAHMS data sets. Namely, we have found out that the resulting cross normalization factors  $f_P$  and  $f_B$  are unrealistically small ( $\approx 0.8$ ) if one takes into account the nucleons measured by PHENIX and BRAHMS collaborations. Both of these factors can be determined directly from the data by dividing the experimental rapidity densities of PHENIX and BRAHMS hadrons by the corresponding ones from STAR collaboration. We have plotted the ratios of average pions and kaons, i.e.  $\pi^+ + \pi^-$  and  $K^+ + K^-$  from PHENIX divided by the corresponding quantities from STAR in fig. 5. As one can see, the experimental ratios mostly lie between 0.9 and 1.0 at all centralities. However, the deviation from unity is clearly large enough so that the previously introduced  $f_P$  must be implemented. In the same figure, we also show the resulting  $f_P$  (thick line) fitted to the STAR+PHENIX+BRAHMS data when excluding protons and anti-protons from PHENIX and BRAHMS. One can see that the fitted  $f_P$  closely follows the experimental ratio of PHENIX and STAR pion rapidity densities. Thus, it seems that the cross-normalization factor for the nucleons would be different and much smaller (0.8 or below) than the cross normalization factor for the pions and kaons. Unfortunately, this cannot be estimated directly from the data, because, unlike for BRAHMS and PHENIX, nucleons from STAR collaboration include all the weak decay products of hyperons. It should be mentioned that both BRAHMS and PHENIX weak feeding corrections at 200A GeV are based on the same PHENIX  $\Lambda$  and  $\bar{\Lambda}$  measurement at 130A GeV. If the underlying assumption of  $\Lambda/p$  being constant at all centralities at all beam energies at RHIC was not correct, then the weak decay corrected proton and anti-proton rapidity densities quoted by PHENIX and BRAHMS would be incorrect as well, which could partly explain the failure of statistical hadronization model fits to the PHENIX and BRAHMS data alone as well as the unrealistically low  $f_P$  and  $f_B$  from fits to the whole data set. In fact, PHENIX

(and BRAHMS) weak decay correction is based on the  $\Lambda^{inc}/p^{excl}=0.89\pm 0.07$  [33] ratio in which  $\Lambda^{inc}$  denotes the inclusive rapidity density of  $\Lambda$  including weak feeding from  $\Xi$ 's and  $\Omega$  while  $p^{excl} = p - 0.64\Lambda^{inc}$  is the rapidity density of protons from which feeding from inclusive  $\Lambda$ 's has been subtracted. This can be compared with the corresponding ratio at 200A GeV measured by the STAR collaboration. In order to estimate the inclusive  $\Lambda$  rapidity density, we sum up all the contributions  $\Lambda^{inc} = \Lambda^{excl} + (\Xi^- \rightarrow \Lambda) + (\Omega \rightarrow \Lambda) + (\Xi^0 \rightarrow \Lambda) = 16.7 + 2.17 + 0.68 \times 0.53/2.0 + \mathcal{O}(2)$ . The  $\Xi^0$  rapidity density is not measured but is expected to be  $\Xi^0 \leq \Xi^-$ . Thus, we get  $\Lambda^{inc}/p^{excl} \approx 21/(34.7 - 0.64 \times 21) \approx 1$ , clearly different from the value obtained by PHENIX collaboration at 130A GeV. For comparison, we note from the table I that the STAR data at 130A GeV suggests that again,  $\Lambda^{inc}/p^{excl} \approx 16.2/(26.4 - 0.64 \times 16.2) \approx 1$ . Because of this significant discrepancy in the  $\Lambda/p$  among the three experiments, we have decided to exclude the proton and anti-proton rapidity densities measured by PHENIX and BRAHMS collaborations in the analysis and all results in this paper are evaluated excluding these 4 measurements. This way, our fitted cross-normalization factors  $f_P$  and  $f_B$  follow the actual ratios of pions and kaons determined from the data and provide more reliable estimate compared with fits including the  $p$  and  $\bar{p}$  from PHENIX and BRAHMS in which cases the low  $\Lambda/p$  ratio would bias the fit towards lower temperatures as well as lower  $f_P$  and  $f_B$ .

We have performed fits to the formula (1) in 7 out of 8 and in 8 out of 11 most central centrality bins at 130 and 200A GeV respectively. There are two reasons why we have refrained from estimating the freeze-out parameters in very peripheral bins. First, the interpolations of lower multiplicity particles, such as hyperons, become less and less accurate going to more peripheral collisions and using only light mesons and nucleons makes the fit unstable, as has been already discussed. Secondly, in extreme peripheral collisions, the role played by exact conservation laws (so-called canonical suppression), especially for multi-strange baryons, may become important. Yet, it is very difficult to make a definite assessment of this effect onto rapidity densities rather than full phase space yields. We remind that at top SPS energy, the difference in  $\Omega$ 's fully integrated yield calculated in grand-canonical and S-canonical (enforcing vanishing net strangeness) ensembles is 32% and 14% with  $N_P$  16 and 40 respectively [19]. Most likely, these figures do not change significantly at RHIC and so it is safer to use the simple grand-canonical formula (1) only when  $N_P \geq 50$ .

#### IV. COMPARISON WITH PREVIOUS ANALYSES

Up to date several statistical hadronization analyses similar to ours have been carried out on RHIC Au-Au collisions. As discussed in the introduction, the majority of them formed ratios of rapidity densities *a posteriori*, thus possibly introducing a bias in the estimation [20]. Also, some of the data we have been using was not yet available. It is then useful to compare our results with previous ones in order to see how much the different input can affect the final result.

In [14], different combinations of ratios of rapidity densities measured by STAR, PHENIX, PHOBOS and BRAHMS collaborations in Au-Au collisions at 130A GeV in 3 centrality bins are analyzed. Depending on the used set of ratios of rapidity densities, the authors find somewhat different chemical freeze-out conditions. In the case of maximal amount of ratios fitted in the analysis, their chemical freeze-out parameters agree with ours within the errors.

STAR collaboration has determined [12, 17] the statistical hadronization model parameters in Au-Au collisions at 200A GeV by using different combinations of ratios of rapidity densities as a function of centrality. Their most recent results are in very good agreement with ours.

The inhomogeneous chemical freeze-out model [15] takes into account possible fluctuations in the temperature and baryon number among created clusters in a collision event. The model has been applied to determine the temperature and baryon chemical potential in Au-Au collisions at 130 and 200A GeV at RHIC. In this analysis, ratios of rapidity densities are implemented and the authors have found out that the choice of ratios included in the analysis can indeed bias the outcome. To try to minimize the bias, particle/antiparticle ratios are included along ratios of various particles and negative pions. The central values of the distributions of temperature and baryon chemical potential are in approximate agreement with our findings.

In [16] ratios of rapidity densities at RHIC energies have been used and the effect of including different sets of rapidity densities as well as ratios of them is explored. Admittedly, the authors find a difference in the fit outcome whether using rapidity densities or ratios or different set of ratios. Among the many quoted results, some are in agreement with ours.

To our knowledge, the only other statistical model analysis [13] which used rapidity densities themselves instead of forming ratios includes the PHENIX  $\pi^\pm$ ,  $K^\pm$ ,  $p$  and  $\bar{p}$  as well as two ratios measured by the STAR collaboration, and finds somewhat lower temperatures than we do, for the same version of the statistical model. We deem that this discrepancy owes to the poorer data set available when that analysis was carried out.

In conclusion, several groups have analyzed the rapidity densities at RHIC 130 and 200A GeV and the results of all groups seem to agree rather well. The resulting baryon chemical potentials agree very well among all groups and seem to be fairly insensitive both to the set of particle species included in the analysis as well as to the details of

the version of the statistical hadronization model. Chemical freeze-out temperature, on the other hand, shows larger discrepancies and seems to be more sensitive to the input data set, which, as has been emphasized, is an effect to be expected in fitting different subsets of ratios, also without including correlations. Finally, the values and behaviour of  $\gamma_S$  as a function of centrality are in very good agreement with previous findings, especially with the ones [14, 17] calculated with the THERMUS [43] package.

On the other hand, we observe a worse fit quality at 200A GeV than generally reported by previous analyses. This difference is certainly owing to our updated and more accurate data set but, again, to some extent this is possibly related to having fitted rapidity densities instead of a subset of ratios.

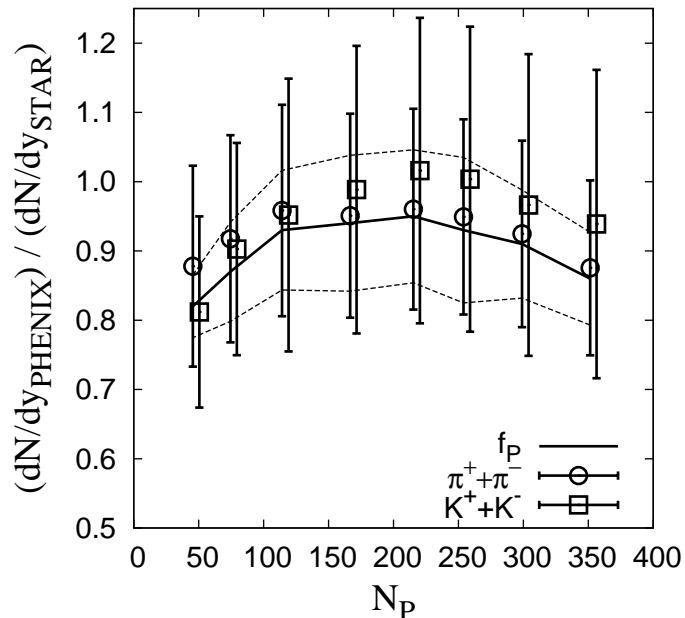


FIG. 5: The average rapidity density of pions (open circles) and kaons (open squares) measured by PHENIX collaboration divided by the same quantity measured by STAR in Au-Au collisions at 200A GeV as a function of centrality. The fitted cross-normalization factor  $f_P$  (thick line) closely follows the measured ratio of pions. Dashed lines visualize the errorband of  $f_P$ .

## V. SUMMARY AND CONCLUSIONS

In summary, we have analyzed within the statistical hadronization model the rapidity densities of various hadron species at mid-rapidity in Au-Au collisions at 130 and 200A GeV measured by STAR, PHENIX and BRAHMS collaborations and determined the relevant statistical hadronization model best fit parameters. This completes our previous analyses at lower center-of-mass energies measured at SPS and AGS.

We have used as input data for the analysis only rapidity densities and not ratios formed out of them because of the bias introduced in fitting subset of ratios. Although a direct comparison is not possible because the data set used in this analysis is the most up-to-date, our results are in general good agreement with those of previous analyses, showing that the effective value of the bias introduced by the actual choice of ratios therein was small and most likely within the fit error.

We have found out that the statistical hadronization model, as implemented by the formula (1) can describe the rapidity densities measured at RHIC relatively well, although discrepancies between data and model are visible and larger than some other groups using ratios in their analyses have reported. This is also reflected in the higher  $\chi^2/dof$  value that we find at  $\sqrt{s_{NN}} = 200$  GeV compared to that at  $\sqrt{s_{NN}} = 130$  GeV. Since the relative deviations between data and model are comparable at both energies, we conclude that the better relative accuracy of measurements at the higher energy has overcome the theoretical accuracy of the simple formula (1). We interpret this not as a failure of the statistical model itself, but an indication that corrections to the simple assumptions underlying formula (1) would be necessary, like those discussed in Sect. III.

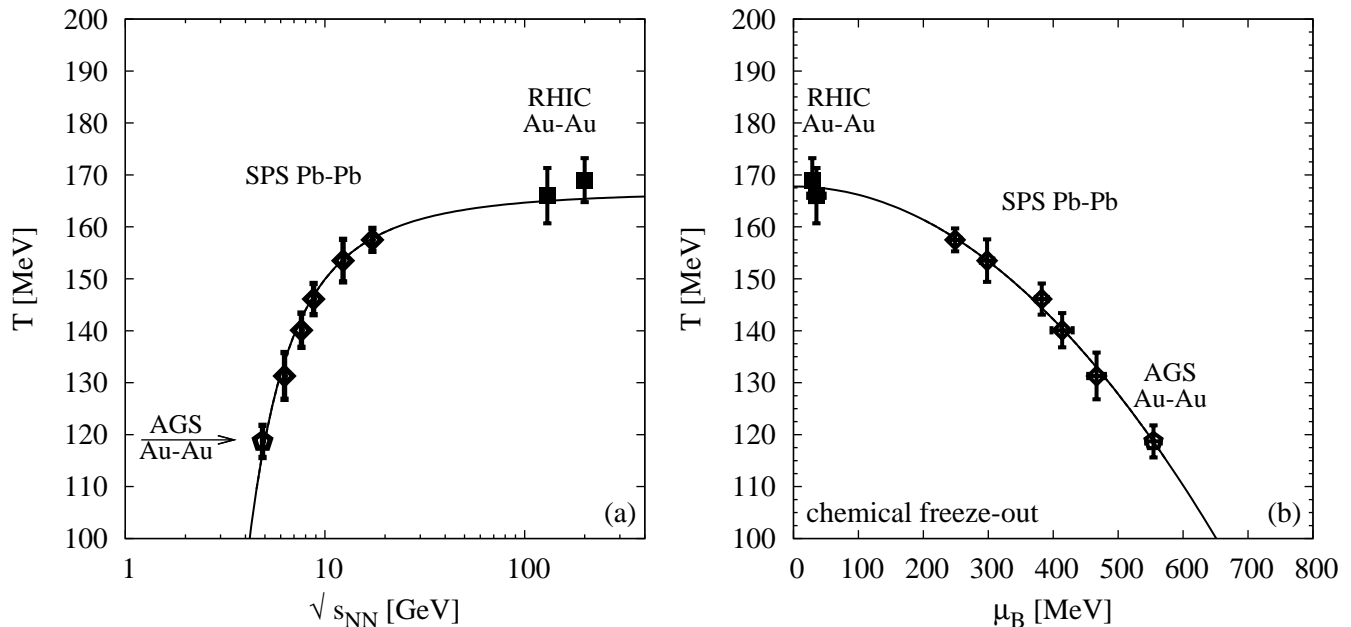


FIG. 6: Chemical freeze-out temperature as a function of center-of-mass energy per participant pair (left panel (a)) and as a function of baryon chemical potential (right panel (b)) in central heavy-ion collisions at AGS, SPS and RHIC. The chemical freeze-out shown in the right panel as well as the curve shown in the left panel are empirical fits to the AGS and SPS points taken from our previous paper [19].

A major result of our analysis is the stability of the temperature as a function of centrality, especially at  $\sqrt{s_{NN}} = 200$  GeV, where all values range from about 166 to 171.4 MeV, hence with an overall spread of around 3%. This confirms previous findings from STAR collaboration.

The strangeness under-saturation parameter increases mildly from peripheral to central collisions where it almost attains 1. Therefore, RHIC data in peripheral collisions demonstrates the phenomenon of phase space under-saturation for mid-rapidity yields. This is also observed in the dependence of normalized  $\phi$  meson yield as a function of centrality [36]: since the temperature is essentially constant, this behaviour can only be parameterized with a  $\gamma_S$  varying as a function of centrality. The authors have recently proposed [44] an explanation of strangeness under-saturation in terms of a superposition of NN collisions and a completely equilibrated hadronic system originated from the central core of the collision, where the Quark Gluon Plasma is formed. Such a scenario will be investigated in more detail in future works.

Finally, we find that the fitted chemical freeze-out temperatures and baryon chemical potentials in central Au-Au collisions nicely fit previously extrapolated curves from lower heavy ion collision energies as shown in fig. 6.

### Acknowledgments

We are greatly indebted with H. Caines and J. H. Chen for their help in using STAR data. We acknowledge stimulating and useful discussions with H. Satz. One of the authors (J.M.) was partly supported by the Academy of Finland, project 114371.

---

### References

- [1] E. Fermi, Prog. Theor. Phys. **5** (1950) 570.
- [2] F. Becattini, Z. Phys. C **69** (1996) 485.
- [3] F. Becattini and U. W. Heinz, Z. Phys. C **76** (1997) 269 [Erratum-ibid. C **76** (1997) 578].
- [4] F. Becattini and G. Passaleva, Eur. Phys. J. C **23** (2002) 551.

- [5] J. Cleymans, H. Satz, E. Suhonen and D. W. von Oertzen, Phys. Lett. B **242** (1990) 111.
- [6] J. Cleymans and H. Satz, Z. Phys. C **57** (1993) 135.
- [7] P. Braun-Munzinger, J. Stachel, J. P. Wessels and N. Xu, Phys. Lett. B **344** (1995) 43.
- [8] F. Becattini, M. Gazdzicki and J. Sollfrank, Eur. Phys. J. C **5** (1998) 143.
- [9] F. Becattini, J. Cleymans, A. Keranen, E. Suhonen and K. Redlich, Phys. Rev. C **64** (2001) 024901.
- [10] A. Mekjian, Phys. Rev. C **17** (1978) 1051; J. Gosset, J.I. Kapusta, and G.D. Westfall, Phys. Rev. C **18** (1978) 844; J. Randrup and S.E. Koonin, Nucl. Phys. A **356** (1981) 223; G. Fai and J. Randrup, Nucl. Phys. A **404** (1983) 551; J. Bondorf, R. Donangelo, I.N. Mishustin, and H. Schulz, Nucl. Phys. A **444** (1985) 460; D.H.E. Gross, A.R. De Angelis, H.R. Jaqaman, P. Jicai and R. Heck, Phys. Rev. Lett. **68** (1992) 146
- [11] A. Baran, W. Broniowski and W. Florkowski, Acta Phys. Polon. B **35** (2004) 779.
- [12] J. Adams *et al.* [STAR Collaboration], Phys. Rev. Lett. **92** (2004) 112301.
- [13] J. Rafelski, J. Letessier and G. Torrieri, Phys. Rev. C **72** (2005) 024905.
- [14] J. Cleymans, B. Kampfer, M. Kaneta, S. Wheaton and N. Xu, Phys. Rev. C **71** (2005) 054901.
- [15] A. Dumitru, L. Portugal and D. Zschesche, Phys. Rev. C **73** (2006) 024902.
- [16] A. Andronic, P. Braun-Munzinger and J. Stachel, Nucl. Phys. A **772** (2006) 167.
- [17] J. Adams *et al.* [STAR Collaboration], Phys. Rev. Lett. **98** (2007) 062301.
- [18] F. Becattini, M. Gazdzicki, A. Keranen, J. Manninen and R. Stock, Phys. Rev. C **69** (2004) 024905.
- [19] F. Becattini, J. Manninen and M. Gazdzicki, Phys. Rev. C **73** (2006) 044905.
- [20] F. Becattini, arXiv:0707.4154 [nucl-th].
- [21] I. G. Bearden *et al.* [BRAHMS Collaboration], Phys. Rev. Lett. **94** (2005) 162301.
- [22] C. Blume [NA49 Collaboration], PoS **HEP2005** (2006) 125 [arXiv:hep-ph/0505137].
- [23] C. Adler *et al.* [STAR Collaboration], Phys. Rev. Lett. **89** (2002) 092301.
- [24] K. J. Eskola, K. Kajantie, P. V. Ruuskanen and K. Tuominen, Nucl. Phys. B **570** (2000) 379.
- [25] D. Kharzeev and M. Nardi, Phys. Lett. B **507** (2001) 121.
- [26] J. Adams *et al.* [STAR Collaboration], Phys. Rev. C **70** (2004) 041901.
- [27] C. Adler *et al.* [STAR Collaboration], Phys. Lett. B **595** (2004) 143.
- [28] J. Adams *et al.* [STAR Collaboration], arXiv:nucl-ex/0311017.
- [29] J. Adams *et al.* [STAR Collaboration], Phys. Rev. Lett. **92** (2004) 182301.
- [30] C. Adler *et al.* [STAR Collaboration], Phys. Rev. C **65** (2002) 041901.
- [31] K. Adcox *et al.* [PHENIX Collaboration], Phys. Rev. Lett. **88** (2002) 242301.
- [32] K. Adcox *et al.* [PHENIX Collaboration], Phys. Rev. C **69** (2004) 024904.
- [33] K. Adcox *et al.* [PHENIX Collaboration], Phys. Rev. Lett. **89** (2002) 092302.
- [34] S. S. Adler *et al.* [PHENIX Collaboration], Phys. Rev. C **69** (2004) 034909; [http://www.phenix.bnl.gov/phenix/WWW/info/data/ppg026\\_data.html](http://www.phenix.bnl.gov/phenix/WWW/info/data/ppg026_data.html).
- [35] B. I. Abelev *et al.* [STAR Collaboration], Phys. Rev. Lett. **99** (2007) 112301.
- [36] J. H. Chen [STAR Collaboration], J. Phys. G **35** (2008) 104053.
- [37] I. Arsene *et al.* [BRAHMS Collaboration], Phys. Rev. C **72** (2005) 014908.
- [38] S. S. Adler *et al.* [PHENIX Collaboration], Phys. Rev. C **72** (2005) 014903.
- [39] J. Adams *et al.* [STAR Collaboration], Phys. Rev. C **71** (2005) 064902.
- [40] J. Adams *et al.* [STAR Collaboration], Phys. Rev. Lett. **97** (2006) 132301.
- [41] W. M. Yao *et al.* [Particle Data Group], J. Phys. G **33** (2006) 1.
- [42] F. Becattini, P. Castorina, J. Manninen and H. Satz, arXiv:0805.0964 [hep-ph], Eur. Phys. J. C in press.
- [43] S. Wheaton and J. Cleymans, arXiv:hep-ph/0407174.
- [44] F. Becattini and J. Manninen, J. Phys. G **35** (2008) 104013, arXiv:0805.0098 [nucl-th].
- [45] Helen Caines, private communication.

## Appendix

centrality	0-6%	6-11%	11-18%	18-26%	26-34%	34-45%	45-58%	58-85%	
$\frac{dN_{h-}}{d\eta}$ [27]	290	236	196	154	115	78.9	47.3	17.9	
$N_P$	352	279	226	172	126	85	47	18	
STAR	$\pi^+$	234±24	190±19	158±16	124±13	92.7±9.3	63.6±6.4	38.1±3.9	<b>1.62±0.4</b> <b>1.28±0.3</b> <b>2.46±0.33</b> <b>2.32±0.31</b>
	$\pi^-$	234±24	190±19	158±16	124±13	92.7±9.3	63.6±6.4	38.1±3.9	
	$p$ [26]	<b>26.37±6.6</b>	<b>21.01±5.3</b>	<b>16.53±4.1</b>	<b>13.03±3.3</b>	<b>10.29±2.6</b>	<b>7.14±1.8</b>	<b>4.36±1.1</b>	
	$\bar{p}$ [26]	<b>18.72±4.7</b>	<b>15.04±3.8</b>	<b>11.85±3.0</b>	<b>9.50±2.4</b>	<b>7.56±1.9</b>	<b>5.35±1.3</b>	<b>3.31±0.8</b>	
	$K^+$ [27]	<b>46.2±6.0</b>	<b>38.0±4.9</b>	<b>28.8±3.8</b>	<b>23.1±3.0</b>	<b>17.2±2.2</b>	<b>11.8±1.5</b>	<b>7.23±0.96</b>	
	$K^-$ [27]	<b>41.9±5.4</b>	<b>34.5±4.5</b>	<b>26.4±3.5</b>	<b>20.8±2.8</b>	<b>15.5±2.0</b>	<b>10.4±1.4</b>	<b>6.48±0.86</b>	
	$\Lambda$	16.2±1.7	12.9±1.3	10.1±1.0	7.34±0.75	5.31±0.62	3.71±0.82	2.23±0.81	
	$\bar{\Lambda}$	11.8±1.2	9.49±0.94	7.52±0.77	5.64±0.57	4.20±0.46	3.01±0.61	1.82±0.61	
	$\phi$	6.26±0.90	5.09±0.67	3.97±0.56	2.77±0.58	1.76±0.64	0.93±0.62	0.43±0.40	
	$\Xi^-$	2.18±0.28	1.74±0.20	1.32±0.17	0.89±0.18	0.53±0.20	0.25±0.17	0.110±0.059	
$\Xi^+$	1.87±0.24	1.47±0.17	1.09±0.14	0.70±0.15	0.38±0.17	0.15±0.15	0.062±0.050		
PHENIX	$\pi^+$	271±35	228±29	186±24	142±19	104±14	69.7±9.0	39.2±6.2	
	$\pi^-$	260±34	214±27	171±22	128±17	93±12	63.0±8.2	38.5±6.0	
	$K^+$	45.4±6.8	37.4±5.5	29.9±4.4	22.2±3.4	15.8±2.5	10.2±1.6	5.5±1.1	
	$K^-$	40.3±6.2	31.1±4.7	23.1±3.5	15.7±2.5	10.4±1.7	6.8±1.1	4.87±0.98	
	$p$	28.1±4.0	22.9±3.1	18.1±2.5	13.3±1.9	9.4±1.4	6.05±0.88	3.43±0.66	
$\bar{p}$	18.4±2.7	15.0±2.1	11.9±1.7	8.8±1.3	6.29±0.97	4.19±0.62	2.52±0.48		
centrality	0-5%	5-10%	10-20%	20-35%	35-75%				
$\frac{dN_{h-}}{d\eta}$ [23]	296.6	243.4	186.7	109.6	33.3				
$\Lambda$ [23] <sup>a</sup>	<b>17.2±1.8</b>	<b>13.2±1.4</b>	<b>10.3±1.0</b>	<b>6.0±0.6</b>	<b>1.63±0.17</b>				
$\bar{\Lambda}$ [23] <sup>a</sup>	<b>12.2±1.3</b>	<b>9.7±1.0</b>	<b>7.5±0.8</b>	<b>4.7±0.5</b>	<b>1.28±0.13</b>				
$\pi^+$ [28]	<b>239±11</b>								
$\pi^-$ [28]	<b>239±11</b>								
centrality	0-11%		11-26%		26-85%				
$\phi$ [30]	<b>5.73±0.78</b>		<b>3.33±0.55</b>		<b>0.98±0.17</b>				
centrality	0-10%		10-25%		25-75%				
$\Xi^-$ [29] <sup>a</sup>	<b>2.02±0.25</b>		<b>1.15±0.17</b>		<b>0.28±0.04</b>				
$\Xi^+$ [29] <sup>a</sup>	<b>1.72±0.21</b>		<b>0.93±0.14</b>		<b>0.22±0.03</b>				
$\Omega + \bar{\Omega}$ [29]	<b>0.56±0.12</b>								
centrality	0-5%	5-15%	15-30%	30-60%	60-92%				
$N_P$	348±10	271.3±8.4	180.2±6.6	78.5±4.6	14.3±3.3				
STAR	$\pi^+$ [32]	<b>276±36</b>	<b>216±28</b>	<b>141±18</b>	<b>57.0±7.4</b>	<b>9.6±1.2</b>			
PHENIX	$\pi^-$ [32]	<b>270±35</b>	<b>200±26</b>	<b>129±17</b>	<b>53.3±6.9</b>	<b>8.6±1.1</b>			
STAR	$K^+$ [32]	<b>46.7±7.2</b>	<b>35±5.5</b>	<b>22.2±3.4</b>	<b>8.3±1.2</b>	<b>0.97±0.19</b>			
PHENIX	$K^-$ [32]	<b>40.5±6.5</b>	<b>30.4±4.8</b>	<b>15.5±2.4</b>	<b>6.2±1.0</b>	<b>0.98±0.18</b>			
STAR	$p$ [32]	<b>28.7±4.1</b>	<b>21.6±3.1</b>	<b>13.2±1.8</b>	<b>5.0±0.7</b>	<b>0.73±0.12</b>			
PHENIX	$\bar{p}$ [32]	<b>20.1±3.0</b>	<b>13.8±2.0</b>	<b>9.2±1.4</b>	<b>3.6±0.5</b>	<b>0.47±0.08</b>			
	$\Lambda$ [33]	<b>17.3±4.4</b>							
	$\bar{\Lambda}$ [33]	<b>12.7±3.4</b>							

<sup>a</sup>Weighted average

TABLE I: Our estimates for the STAR (top panel) and PHENIX (middle panel) rapidity densities of various hadron species in different centrality windows in Au-Au collisions at 130A GeV. STAR  $K^\pm$ ,  $p$  and  $\bar{p}$  are experimental values while all others are derived from the measured values shown bold face in the bottom part of the table by interpolation described in Section II A. The STAR pion rapidity densities are corrected for weak decays while all other rapidity densities include the weak decay products (if any) of weakly decaying resonances.

	centrality $N_P$	0-5%	5-10%	10-15%	10-20%	15-20%
		351.4±2.9	299.0±3.8	253.9±4.3	235±9	215.3±5.3
S T A R	$\pi^+$ [12, 45]	<b>322.2±19.2</b>	<b>257.0±15.2</b>	210.8±12.7	<b>193.8±11.4</b>	176.6±10.7
	$\pi^-$ [12, 45]	<b>327.0±19.5</b>	<b>260.7±15.4</b>	213.7±12.8	<b>196.1±11.6</b>	178.7±10.8
	$K^+$ [12, 45]	<b>51.27±5.92</b>	<b>40.82±4.25</b>	32.9±3.2	<b>29.97±2.86</b>	27.0±2.6
	$K^-$ [12, 45]	<b>49.47±5.71</b>	<b>39.78±4.15</b>	31.7±3.1	<b>28.74±2.74</b>	25.8±2.4
	$p$ [12, 45]	<b>34.70±4.10</b>	<b>28.23±2.99</b>	22.0±2.2	<b>20.12±1.94</b>	18.3±1.7
	$\bar{p}$ [12, 45]	<b>26.70±3.15</b>	<b>21.42±2.27</b>	17.1±1.7	<b>15.69±1.51</b>	14.3±1.4
	$\Lambda$ [17]	<b>16.7±1.1</b>	13.55±0.91	11.02±0.77	<b>10.0 ±0.7</b>	8.98±0.64
	$\bar{\Lambda}$ [17]	<b>12.7±0.9</b>	10.36±0.69	8.47±0.56	<b>7.7 ±0.5</b>	6.93±0.46
	$\Xi^-$ [17]	<b>2.17±0.20</b>	1.86±0.14	1.55±0.11	<b>1.41±0.09</b>	1.268±0.074
	$\Xi^+$ [17]	<b>1.83±0.21</b>	1.52±0.14	1.25±0.11	<b>1.14±0.09</b>	1.027±0.075
$\phi$ [35, 36, 45]	<b>7.95±0.74</b>	6.81±0.73	5.89±0.53	<b>5.37±0.51</b>	4.82±0.51	
$\Omega + \bar{\Omega}$ [17]	<b>0.53±0.06</b>	0.445±0.044	0.368±0.035		0.299±0.030	
P	$\pi^+$ [34]	<b>286.4±24.2</b>	<b>239.6±20.5</b>	<b>204.6±18.0</b>		<b>173.8±15.6</b>
H	$\pi^-$ [34]	<b>281.8±22.8</b>	<b>238.9±19.8</b>	<b>198.2±16.7</b>		<b>167.4±14.4</b>
E	$K^+$ [34]	<b>48.9±6.3</b>	<b>40.1±5.1</b>	<b>33.7±4.3</b>		<b>27.9±3.6</b>
N	$K^-$ [34]	<b>45.7±5.2</b>	<b>37.8±4.3</b>	<b>31.1±3.5</b>		<b>25.8±2.9</b>
I	$p$ [34]	<b>18.4±2.6</b>	<b>15.3±2.1</b>	<b>12.8±1.8</b>		<b>10.6±1.5</b>
X	$\bar{p}$ [34]	<b>13.5±1.8</b>	<b>11.4±1.5</b>	<b>9.5±1.3</b>		<b>7.9±1.1</b>
B	$\pi^+$	309.8±32.3	256.8±25.2	213.7±21.3	<b>196.2±19.7</b>	178.8±18.2
R	$\pi^-$	302.6±31.6	253.2±24.9	212.2±21.2	<b>195.3±19.6</b>	178.4±18.2
A	$K^+$	49.8±5.2	40.2±4.0	32.7±3.3	<b>29.8±3.0</b>	26.9±2.8
H	$K^-$	44.7±4.7	37.1±3.7	30.7±3.1	<b>28.1±2.9</b>	25.5±2.6
M	$p$	20.0±2.1	17.2±1.7	14.6±1.5	<b>13.4±1.4</b>	12.2±1.3
S	$\bar{p}$	14.8±1.6	12.6±1.2	10.6±1.1	<b>9.7±1.0</b>	8.8±0.9
	centrality $N_P$	0-10%				
		328±6				
B	$\pi^+$ [37]	<b>283.3±28.4</b>				
R	$\pi^-$ [37]	<b>277.9±27.9</b>				
A	$K^+$ [37]	<b>45.0±4.55</b>				
H	$K^-$ [37]	<b>40.9±4.14</b>				
M	$p$ [37]	<b>18.6±1.87</b>				
S	$\bar{p}$ [37]	<b>13.7±1.38</b>				

TABLE II: Rapidity densities of various hadrons in Au-Au collisions at 200A GeV in different centrality windows. Bold face numbers denote measured values while numbers written with standard fonts denote our estimates. Our estimates are interpolated from the experimental values as described in the Sect II A. The STAR  $p$  and  $\bar{p}$  rapidity densities do include weak feeding from (multi)strange hyperons while PHENIX and BRAHMS  $p$  and  $\bar{p}$  rapidity densities include feeding from  $\Sigma$ 's only. All other rapidity densities in this table are corrected for the weak feeding (if relevant).

	centrality N <sub>P</sub>	20-30%	30-40%	40-50%	50-60%	60-70%	70-80%
		166.6±5.4	114.2±4.4	74.4±3.8	45.5±3.3	25.7±3.8	13.4±3.0
S T A R	$\pi^+$ [12, 45]	<b>134.93±7.78</b>	<b>89.24±5.13</b>	<b>58.66±3.35</b>	<b>36.24±2.07</b>	<b>21.07±1.20</b>	
	$\pi^-$ [12, 45]	<b>136.07±7.84</b>	<b>89.64±5.16</b>	<b>58.85±3.36</b>	<b>36.33±2.07</b>	<b>21.13±1.20</b>	
	$K^+$ [12, 45]	<b>20.48±1.77</b>	<b>13.61±1.11</b>	<b>8.690±0.680</b>	<b>5.400±0.410</b>	<b>2.980±0.220</b>	
	$K^-$ [12, 45]	<b>19.68±1.70</b>	<b>13.18±1.07</b>	<b>8.370±0.660</b>	<b>5.190±0.390</b>	<b>2.890±0.220</b>	
	$p$ [12, 45]	<b>14.39±1.26</b>	<b>9.300±0.760</b>	<b>6.170±0.480</b>	<b>3.880±0.290</b>	<b>2.200±0.160</b>	
	$\bar{p}$ [12, 45]	<b>11.180±0.980</b>	<b>7.460±0.610</b>	<b>4.930±0.390</b>	<b>3.160±0.240</b>	<b>1.840±0.140</b>	
	$\Lambda$	6.67±0.47	4.39±0.34	2.71±0.21	1.42±0.16		
	$\bar{\Lambda}$	5.18±0.35	3.43±0.27	2.13±0.17	1.15±0.12		
	$\Xi^-$	0.903±0.037	0.537±0.031	0.315±0.025	0.205±0.035		
	$\Xi^+$	0.756±0.043	0.484±0.037	0.295±0.029	0.165±0.031		
$\phi$ [35, 36, 45]	<b>3.47±0.44</b>	<b>2.29±0.23</b>	<b>1.44±0.14</b>	<b>0.810±0.092</b>	<b>0.450±0.051</b>	<b>0.20±0.022</b>	
$\Omega + \bar{\Omega}$	0.213±0.025	0.127±0.020	0.073±0.011	0.053±0.015			
P	$\pi^+$ [34]	<b>130.3±12.4</b>	<b>87.0±8.6</b>	<b>54.9±5.6</b>	<b>32.4±3.4</b>	<b>17.0±1.8</b>	<b>7.9±0.8</b>
H	$\pi^-$ [34]	<b>127.3±11.6</b>	<b>84.4±8.0</b>	<b>52.9±5.2</b>	<b>31.3±3.1</b>	<b>16.3±1.6</b>	<b>7.7±0.7</b>
E	$K^+$ [34]	<b>20.6±2.6</b>	<b>13.2±1.7</b>	<b>8.0±0.8</b>	<b>4.5±0.4</b>	<b>2.2±0.2</b>	<b>0.89±0.09</b>
N	$K^-$ [34]	<b>19.1±2.2</b>	<b>12.3±1.4</b>	<b>7.4±0.6</b>	<b>4.1±0.4</b>	<b>2.0±0.1</b>	<b>0.88±0.09</b>
I	$p$ [34]	<b>8.1±1.1</b>	<b>5.3±0.7</b>	<b>3.2±0.5</b>	<b>1.8±0.3</b>	<b>0.93±0.15</b>	<b>0.40±0.07</b>
X	$\bar{p}$ [34]	<b>5.9±0.8</b>	<b>3.9±0.5</b>	<b>2.4±0.3</b>	<b>1.4±0.2</b>	<b>0.71±0.12</b>	<b>0.29±0.05</b>
B R A H M S	$\pi^+$	139.2±13.9	100.2±11.4	67.1±9.3	27.9±7.7		
	$\pi^-$	138.9±13.9	98.7±11.2	64.0±9.1	27.7±7.7		
	$K^+$	20.8±2.1	15.1±1.8	10.0±1.5	2.7±1.3		
	$K^-$	19.4±2.0	13.3±1.6	8.4±1.4	3.4±1.2		
	$p$	9.22±0.93	5.98±0.71	3.61±0.58	2.02±0.54		
	$\bar{p}$	6.70±0.68	4.50±0.53	2.86±0.46	1.58±0.42		
	centrality N <sub>P</sub>	20-40%		40-60%		60-80%	
		141±8		62±9		21±6	
S T A R	$\Lambda$ [17]	<b>5.53±0.39</b>		<b>2.07±0.14</b>		<b>0.58±0.04</b>	
	$\bar{\Lambda}$ [17]	<b>4.30±0.30</b>		<b>1.64±0.11</b>		<b>0.48±0.03</b>	
	$\Xi^-$ [17]	<b>0.72±0.03</b>		<b>0.26±0.02</b>		<b>0.063±0.005</b>	
	$\Xi^+$ [17]	<b>0.62±0.04</b>		<b>0.23±0.02</b>		<b>0.061±0.004</b>	
	$\Omega + \bar{\Omega}$ [17]	<b>0.17±0.02</b>		<b>0.063±0.009</b>			
B R A H M S	$\pi^+$ [37]	<b>119.7±12.1</b>		<b>47.5±4.85</b>			
	$\pi^-$ [37]	<b>118.8±12.0</b>		<b>46.3±4.71</b>			
	$K^+$ [37]	<b>17.9±1.83</b>		<b>6.3±0.68</b>			
	$K^-$ [37]	<b>16.3±1.7</b>		<b>5.9±0.64</b>			
	$p$ [37]	<b>7.6±0.77</b>		<b>2.81±0.29</b>			
	$\bar{p}$ [37]	<b>5.6±0.6</b>		<b>2.22±0.24</b>			

TABLE III: Rapidity densities of various hadrons in Au-Au collisions at 200A GeV in different centrality windows. Bold face numbers denote measured values while numbers written with standard fonts denote our estimates. Our estimates are interpolated from the experimental values as described in the Sect II A. The weak decay corrections are the same as listed in the previous table.

centrality	$T$ [MeV]	$\mu_B$ [MeV]	$\gamma_S$	$dV/dy$ [fm <sup>3</sup> ]	$\chi^2/dof$	$f_P$
STAR 130A GeV best fit parameters						
0-6%	165.9±5.3	35.1±12.6	1.109±0.078	1097±258	5.9 / 7	
6-11%	165.3±5.1	34.0±12.2	1.104±0.075	925±211	5.4 / 7	
11-18%	165.3±5.3	33.2±12.6	1.053±0.075	760±176	6.1 / 7	
18-26%	162.5±5.4	30.7±13.3	0.977±0.078	712±173	2.6 / 7	
26-34%	163.1±2.5	28.1±15.0	0.907±0.056	534±61	1.4 / 7	
34-45%	161.1±7.4	27.3±21.8	0.863±0.091	410±140	2.5 / 7	
45-58%	153.5±7.8	26.9±26.1	0.823±0.096	352±136	4.7 / 7	
PHENIX 130A GeV best fit parameters						
0-5%	161.4±6.9	33.9±16.8	1.02±0.16	1397±475	1.7 / 2	
STAR+PHENIX 130A GeV best fit parameters						
0-6%	163.8 ±4.1	36.3 ±10.2	1.109 ±0.067	1225 ±228	8.2 / 12	0.919±0.067
6-11%	163.7 ±4.0	36.1 ±9.91	1.097 ±0.064	1013 ±182	8.6 / 12	0.911±0.065
11-18%	163.8 ±4.0	35.9 ±10.1	1.043 ±0.064	833 ±150	10.3 / 12	0.897±0.065
18-26%	161.9 ±3.9	34.4 ±10.7	0.954 ±0.024	750 ±133	7.2 / 12	0.844±0.060
26-34%	162.1 ±4.4	32.9 ±5.26	0.884 ±0.067	576 ±116	7.1 / 12	0.801±0.061
34-45%	159.1 ±4.9	32.7 ±13.6	0.827 ±0.071	460 ±106	7.5 / 12	0.798±0.064
45-58%	153.3 ±5.4	26.8 ±18.3	0.813 ±0.080	357 ±96	5.0 / 12	0.841±0.018

TABLE IV: Statistical hadronization model best fit parameters at chemical freeze-out in Au-Au collisions at 130A GeV.

centrality	$T$ [MeV]	$\mu_B$ [MeV]	$\gamma_S$	$dV/dy$ [fm <sup>3</sup> ]	$\chi^2/dof$	$f_P$	$f_B$
STAR 200A GeV best fit parameters							
0-5%	168.0±6.2	28.8±14.3	0.935±0.064	1419±377	22.2 / 8		
5-10%	169.5±6.8	29.1±14.7	0.941±0.069	1055±304	26.8 / 8		
10-15%	167.0±7.3	26.8±16.2	0.979±0.079	941±296	36.9 / 8		
10-20%	168.8±6.0	27.0±13.3	1.054±0.077	745±190	22.4 / 7		
15-20%	167.8±7.0	27.1±15.3	0.971±0.076	750±225	36.1 / 8		
20-30%	169.2±6.3	27.9±12.5	0.954±0.064	537±141	30.0 / 8		
30-40%	166.4±5.5	22.0±12.7	0.951±0.063	399±95	26.7 / 8		
40-50%	165.8±5.2	21.4±12.8	0.900±0.059	274±62	25.1 / 8		
50-60%	164.9±3.1	20.5±8.0	0.902±0.043	173±24	7.0 / 8		
STAR+PHENIX+BRAHMS 200A GeV best fit parameters							
0-5%	169.2±5.2	29.5±11.2	0.929±0.044	1336±302	23.4 / 14	0.863±0.073	0.89±0.12
5-10%	171.2±5.2	29.7±11.3	0.928±0.048	976±210	28.1 / 14	0.912±0.078	0.931±0.082
10-15%	168.9±5.5	27.6±12.6	0.960±0.054	868±201	39.7 / 14	0.928±0.093	0.932±0.096
15-20%	169.9±5.4	27.9±12.0	0.951±0.051	686±156	38.9 / 14	0.948±0.095	0.944±0.098
20-30%	171.4±5.0	28.8±9.90	0.935±0.046	489±102	32.8 / 14	0.942±0.088	0.970±0.091
30-40%	168.3±4.4	23.1±10.2	0.930±0.043	367±68	30.0 / 14	0.931±0.085	1.04±0.10
40-50%	167.3±3.1	22.5±9.35	0.883±0.030	257±34	27.9 / 14	0.870±0.068	1.06±0.12
50-60%	166.2±3.3	20.8±10.4	0.874±0.045	165±24	11.1 / 14	0.818±0.051	0.67±0.11

TABLE V: Statistical hadronization model best fit parameters at chemical freeze-out in Au-Au collisions at 200A GeV. Errors are scaled according to the PDG scaling scheme [41] by a factor  $\sqrt{\chi^2/dof}$ .

	Experiment (E)	Model (M)	Residual	(M - E)/E (%)
STAR Au-Au 130A GeV 0-6% most central collisions				
$\pi^+$	234±24	213	-0.87	-8.93
$\pi^-$	234±24	215	-0.76	-7.82
$K^+$	46.2±6.0	49.0	0.46	5.96
$K^-$	41.9±5.4	45.7	0.69	8.95
$p$	26.4±5.8	32.2	1.0	22.3
$\bar{p}$	18.7±4.1	22.4	0.90	19.8
$\phi$	6.26±0.90	6.61	0.38	5.48
$\Lambda$	16.2±1.6	16.3	0.064	0.648
$\bar{\Lambda}$	11.8±1.2	12.2	0.32	3.28
$\Xi^-$	2.18±0.28	2.00	-0.63	-8.24
$\bar{\Xi}^+$	1.87±0.24	1.59	-1.2	-14.9

TABLE VI: Comparison between estimated rapidity densities in the combined fit and rapidity densities measured by STAR in central Au-Au collisions at 130A GeV. The 3rd and 4th column show the discrepancy between data and model in units of standard error and in percentages, respectively.

	Experiment (E)	Model (M)	Residual	(M - E)/E (%)
STAR Au-Au 200A GeV 0-5% most central collisions				
$\pi^+$	322±19	326	0.21	1.24
$\pi^-$	327±20	328	0.055	0.326
$K^+$	51.3±5.9	57.1	0.99	11.4
$K^-$	49.5±5.7	53.9	0.78	8.97
$p$	34.7±4.1	41.8	1.7	20.4
$\bar{p}$	26.7±3.1	30.9	1.3	15.9
$\phi$	7.95±0.74	6.73	-1.6	-15.3
$\Lambda$	16.7±1.1	14.4	-2.1	-13.9
$\bar{\Lambda}$	12.70±0.92	11.07	-1.8	-12.8
$\Xi^-$	2.17±0.20	2.02	-0.74	-6.86
$\bar{\Xi}^+$	1.83±0.21	1.67	-0.76	-8.51
$\Omega + \bar{\Omega}$	0.530±0.057	0.651	2.1	22.9

TABLE VII: Comparison between estimated rapidity densities in the combined fit and rapidity densities measured by STAR in central Au-Au collisions at 200A GeV. The 3rd and 4th column show the discrepancy between data and model in units of standard error and in percentages, respectively.